This article was downloaded by: [171.67.216.21]
On: 26 April 2014, At: 13:17
Publisher: Taylor & Francis
Informa Ltd Registered in England and Wales Registered Number: 1072954 Registered office: Mortimer House, 37-41 Mortimer Street, London W1T 3JH, UK

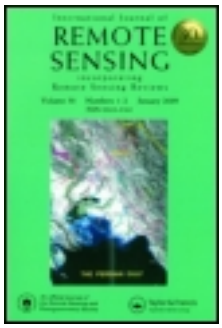

International Journal of Remote Sensing
Publication details, including instructions for authors and subscription information:
http://www.tandfonline.com/loi/tres20

Urban heat island

H. H. KIM [a]
[a] Laboratory for Terrestrial Physics, NASA-Goddard Space Flight Center , Greenbelt, MD 20771, U.S.A.
Published online: 03 Apr 2007.

To cite this article: H. H. KIM (1992) Urban heat island, International Journal of Remote Sensing, 13:12, 2319-2336, DOI: 10.1080/01431169208904271

To link to this article: http://dx.doi.org/10.1080/01431169208904271

PLEASE SCROLL DOWN FOR ARTICLE

Taylor & Francis makes every effort to ensure the accuracy of all the information (the "Content") contained in the publications on our platform. However, Taylor & Francis, our agents, and our licensors make no representations or warranties whatsoever as to the accuracy, completeness, or suitability for any purpose of the Content. Any opinions and views expressed in this publication are the opinions and views of the authors, and are not the views of or endorsed by Taylor & Francis. The accuracy of the Content should not be relied upon and should be independently verified with primary sources of information. Taylor and Francis shall not be liable for any losses, actions, claims, proceedings, demands, costs, expenses, damages, and other liabilities whatsoever or howsoever caused arising directly or indirectly in connection with, in relation to or arising out of the use of the Content.

This article may be used for research, teaching, and private study purposes. Any substantial or systematic reproduction, redistribution, reselling, loan, sub-licensing, systematic supply, or distribution in any form to anyone is expressly forbidden. Terms & Conditions of access and use can be found at http://www.tandfonline.com/page/terms-and-conditions

INT. J. REMOTE SENSING, 1992, VOL. 13, NO. 12, 2319–2336

Urban heat island

H. H. KIM

Laboratory for Terrestrial Physics, NASA-Goddard Space Flight Center, Greenbelt, MD 20771, U.S.A.

(Received 14 March 1991)

Abstract. The phenomenon of an urban heat island was investigated by the use of Landsat/Thematic Mapper data sets collected over the metropolitan area of Washington, DC. By combining the derived spectral albedos and temperatures, surface energy composites of five surface categories were analysed. The results indicate that urban heating is attributable to a large excess in heat from the rapidly heating urban surfaces consisting of buildings, asphalt, bare-soil and short grasses. In summer, the symptoms of diurnal heating begin to appear by mid-morning and can be about 10°C warmer than nearby woodlands.

Downloaded by [171.67.216.21] at 13:17 26 April 2014

1. Introduction

History shows that man has steadily changed the Earth's surface. Had Christopher Columbus and his crew landed on the shores of mainland U.S.A. instead of the West Indies, they would have witnessed the sight of endless sandy beaches and immense primeval forests as far as the eye could behold. Some five hundred years later, today's air travellers from the Atlantic find that the entire East coast, from Cape Cod to northern Virginia, is essentially made up of a repetition of big and small cities as the entire stretch is in the process of being transformed into a gigantic megapolis.

Some changes have taken place at a relatively slow pace, but modern urbanization is a case of rapid changes where man has created his habitat and found degrees of discomfort by the accompanying climate changes. For example, the residents of cities in tropical and temperate zones often experience a regional climate phenomon known as an urban heat island. The temperature within an urban area tends to be much warmer than its rural counterpart.

Historically, such climatic changes brought on by large scale deforestation have been noted from the time of the early settlers in North America including Thomas Jefferson in 1824 (Thompson 1981). However, the climatic alterations in early years were imperceptible. Perceptible changes began to surface as the result of a dynamic growth in urban populations after World War II. Accordingly interesting climatological studies in conjunction with urban growth are found in the works by Duckworth and Sandberg (1954), Landsberg (1970, 1972), Oke (1976), Oke *et al.* (1972), Terjung *et al.* (1975), Carlson *et al.* (1981), Carlson (1986) and Abedayo (1987, 1990). The works by Landsberg and Maisel (1972), Harneck and Landsburg (1975) and Viterito (1989) dealt with the urban heating phenomena in metropolitan Washington, DC.

In this study, the phenomenon of an urban heat island is investigated by the use of Landsat/Thematic Mapper (TM) data collected seasonally over metropolitan

0143–1161/92 $3.00 © 1992 Taylor & Francis Ltd

Washington, DC. This paper will examine the changes being brought on by urbanization and elucidate the causes of urban heating (Kim 1991). For this purpose, the net solar radiation absorbed by several surface categories will be compared and followed through their transformations into different forms of thermal energies in an attempt to establish energy balance.

2. Surface energy balance

In the scheme of surface energy balance, the net solar radiation absorbed becomes the driving force in land processes. Therefore, the phenomenon of an urban heat island will, first, be investigated from the aspect of selective absorptions taking place at the surface. Then the transformation of the absorbed solar energy will be analyzed from the aspect of selective heating.

In order to simplify the matter, the transformation of the solar energy at the surface will be considered in one-dimension ignoring any horizontal energy transport. At the same time, the transfer processes will be strictly limited to the surface phenomena disregarding any subsequent warming or cooling effects by the atmosphere above or the bulk material below. Under these conditions, the net all-wavelength radiation balance, $R_{(bal)}$, can be given as a balance between the shortwave radiation intake (SRI) and the Earth's thermal energy. The relation is given in the following expression:

$$R_{(bal)} = SRI - OLR - H_{(sens)} - LE \tag{1}$$

Where: OLR = Outgoing longwave radiation, $H_{(sens)}$ = Sensible heat flux, LE = Latent heat of evaporation.

Since multi-spectral data are being applied, the SRI is the sum of all shortwave spectral channels.

$$SRI = \sum_{i=1} F_i^{(g)} * (1 - \rho_i) \tag{2}$$

where: $F_i^{(g)}$ = the down-welling flux at the ground in spectral channel i, ρ_i = the reflectance of a spectral channel i.

Unfortunately present satellite systems are not designed for the purpose of measuring surface energy balance, especially at high spatial resolution. For instance, even though the present TM system does provide an almost complete coverage of the solar spectrum, there are sizeable gaps in the near-IR coverage. Furthermore the present Landsat's Sun-synchronous orbital coverage is configured so that it can provide mid-morning coverage of a site whereas full blown urban heating does not develop until mid-afternoon.

Interpolation and augmentation were needed to stretch the TM's performance. For instance, an additional spectral channel was created to fill the spectral coverage gap between 0·9 and 1·65 μm by smoothing the spectral response curves (see Appendix A). In order to obtain the amplitudes of diurnal heating, pre-dawn wet-bulb temperature readings of the National Weather Service were added to supplement the 9.33 am readings of TM band-6.

3. Derivation of spectral albedos

Satellite data application to the urban heat island phenomenon has become possible only since the recent advent of reliable spectral albedo measurements. Spectral albedos are important initial inputs needed for the formulation of surface

Downloaded by [171.67.216.21] at 13:17 26 April 2014

energy balance. For the satellite data derivation of spectral albedo, an atmospheric solar radiation model in conjunction with a surface albedo model or ground based measurements (Nunez *et al.* 1987), are needed. A practical method which converts the radiances of the remotely-sensed data to reflectance terms was introduced in previous work by the author (Kim and Elman 1990). The procedure involves finding a best fit atmosphere out of many atmospheres modelled and stored in convenient 3 by 3 matrix format. After a best fit atmosphere for a desired scene is found, that particular atmosphere is invoked for pixel by pixel atmospheric correction of the scene.

Finding a suitable atmosphere is always a problem as it requires knowledge of the aerosols in the atmosphere. Specific parametric data required are values of the aerosol density in columnar volume, n, and the Jungean size distribution patterns of the aerosols, v^*. The technique of inferring the above aerosol parameters without the help of ground based measurements, is based on finding sets of recognizable dark targets in the imagery. This dark pixel method indicates the upwelling radiance from low reflectance targets is primarily of atmospheric origin. A dual dark pixel method being applied here pertains to the fact that radiances from two wavelengths, one in the shortwavelength blue region and the other in the near-IR region are applied in order to characterize the wavelength dependency of the aerosol size distribution. For instance, the radiances from an area of the Potomac River in the near-IR region and a golf course in the blue region were identified as candidates.

Since sets of multi-spectral data are available, additional refinement in inferring the aerosol parameters can be achieved by checking the conformity to the Lambertian assumption. The low reflectances of dark surfaces are associated with large absorptions and their directional patterns are likely to obey the cosine law. Thus the raw radiances of the grass and water are plotted against the Lambertian assumption as shown in the polar plots of figure 1. Deviations from the Lambertian circle can be constructed as a measure of atmospheric effects.

In table 1, aerosol parameters being inferred from the golf course grass in the *East Potomac River Park* and a section of the *Potomac River* are listed. Uncorrected raw radiances and Lambertian reflectances in per cent are given in the fourth and fifth columns respectively. The sixth to eighth columns pertain to aerosol densities in columnar volume, in numbers of particles per cm^2, their size Jungean size parameters, v^*, and corresponding τ_{Mie} values for bands 1 and 4. Attained reflectances after the correction are listed in the last column and this column should be compared against desired Lambertian reflectances given in the fifth column.

In figure 2 derived reflectances of the grass and water after the atmospheric corrections are presented along with respective Lambertian values.

4. Training sites within the urban area

In a micro-scale study such as this, a single TM scene with a variety of surface types can become an adequate source of data. A TM scene encompasses an area of 185 km by 185 km and the District of Columbia proper occupies an area of approximately 15 km by 10 km. Yet within the metropolis are the Mall, numerous parks, rivers, building, and large boulevards lined with deciduous trees. Such diversity is convenient but it tends to modify the generic meaning of a core urban setting. Therefore a section of downtown Washington, DC, was set aside as a core urban site. Then four additional training sites were selected to represent other surface

Downloaded by [171.67.216.21] at 13:17 26 April 2014

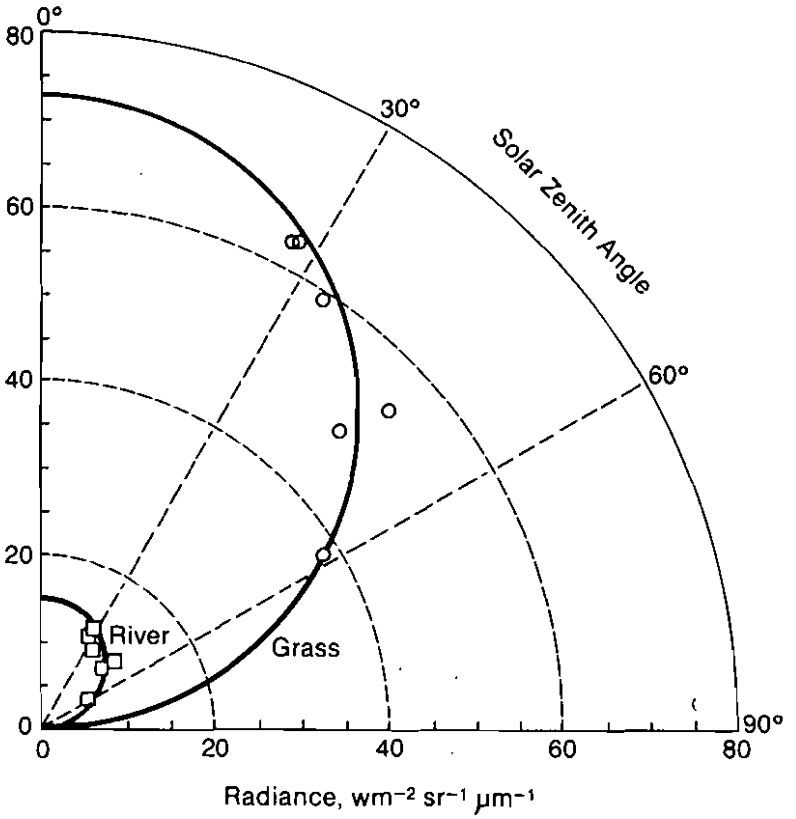

Figure 1. Raw radiances from grass and water. Heavy dark lines are radiances which satisfy the Lambertian assumption.

Table 1. Aerosol parameters for atmospheric effects correction.

Date	SZA (deg)	Bands	Digital counts	Lamb. refl. (%)	n ($\times 10^8$)	v*	τ_{Mie}	Achieved refl. (%)
2 November 1982	58	1	63·5	2·36	4·87	3·0	0·29	2·46
		4	10·0	1·57			0·14	1·67
18 March 1989	47	1	89·49	3·02	10·3	3·0	0·32	2·83
		4	16·17	2·01			0·21	2·63
24 March 1984	44	1	80·8	3·16	6·23	3·0	0·31	3·14
		4	13·0	2·1			0·16	2·01
9 August 1989	34	1	93·3	3·75	6·23	3·4	0·23	4·11
		4	14·9	2·5			0·11	2·39
26 May 1985	28	1	105·3	3·97	10·3	3·4	0·38	3·98
		4	18·0	2·64			0·18	2·52
24 June 1987	27	1	105·0	3·99	10·3	3·6	0·38	3·94
		4	17·0	2·66			0·13	2·76

Downloaded by [171.67.216.21] at 13:17 26 April 2014

categories within the city. The locations and characteristics of the five training sites are described below.

1. *City blocks*: An area of 8·6 km^2 (9526 pixels), largely made up of business buildings and asphalt surfaces was used to represent a core city area. However, many of the streets in Washington, DC, are wide and lined with large deciduous trees along both sides.
2. *Bare soil*: 681 pixels of a land fill site in suburban Bowie, MD, was selected as a bare soil target. The soil is clay loam and the site is constantly being bulldozed and raked over to bury refuse. Therefore the surface is liberally littered with papers, plastic and miscellaneous items but is practically void of any vegetation.
3. *Short grass*: East Potomac Park is an island in the Potomac River and most of the island is occupied by a golf course. This year round golf course is covered with well-manicured short grass and the average height is about 10 cm. A section of the island is represented by 882 pixels.
4. *Forest*: A stretch of woodland (6508 pixels) known as Rock Creek Park extends for several kilometres in a north-south direction. During the growing season, a mix of deciduous and conifers fully cover the uneven terrain in which a small creek runs. The average height of the canopy, a mixture of oak, pine and maples, ranges from 15 to 20 m.

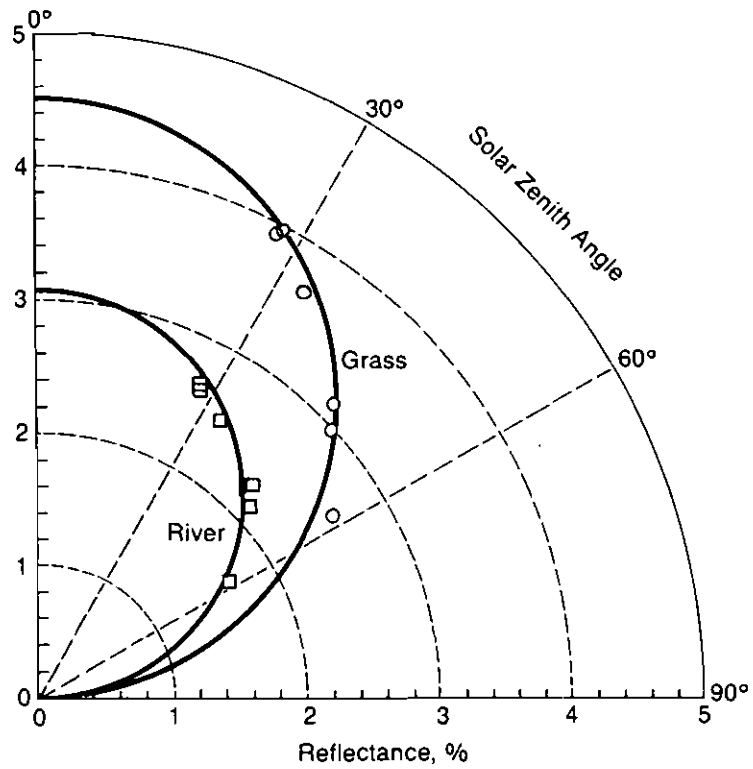

Figure 2. Derived reflectances after atmospheric correction measures were applied.

Downloaded by [171.67.216.21] at 13:17 26 April 2014

Table 2. Derived spectral reflectances of an urban area.

Date	SZA (deg)	TM bands						
		B1	B2	B3	B4	B4-5	B5	B7
2 November 1982	57·8	4·8	5·9	6·0	10·6	9·0	7·5	9·6
18 March 1989	47·6	6·2	7·5	7·6	13·4	11·5	9·5	12·2
24 March 1984	44·9	6·5	7·8	8·0	14·1	12·0	9·9	12·6
9 August 1989	33·3	7·6	9·3	9·5	16·7	14·2	11·8	15·1
26 May 1985	27·9	8·1	9·8	10·0	17·7	15·1	12·5	16·0
24 June 1987	27·3	8·1	9·9	10·1	17·8	15·2	12·5	16·1

5. *Potomac River*: A section of the Potomac River (9850 pixels) became the source of water signatures.

In this text, albedos are given in terms of spectral reflectance. Reflectances, in percentage, are defined by the phase angles of the incident sunlight and the viewers. Spectral reflectances of the five surfaces above were derived for six data sets and a sample of spectral reflectances pertaining to city blocks are presented in table 2. Spectral features from 9 August 1989, data are illustrated in figure 3. The reflectances are for nadir view and the curves are given in cm^{-1} to offer an energy perspective of the net solar insolation. The object of deriving spectral reflectances is

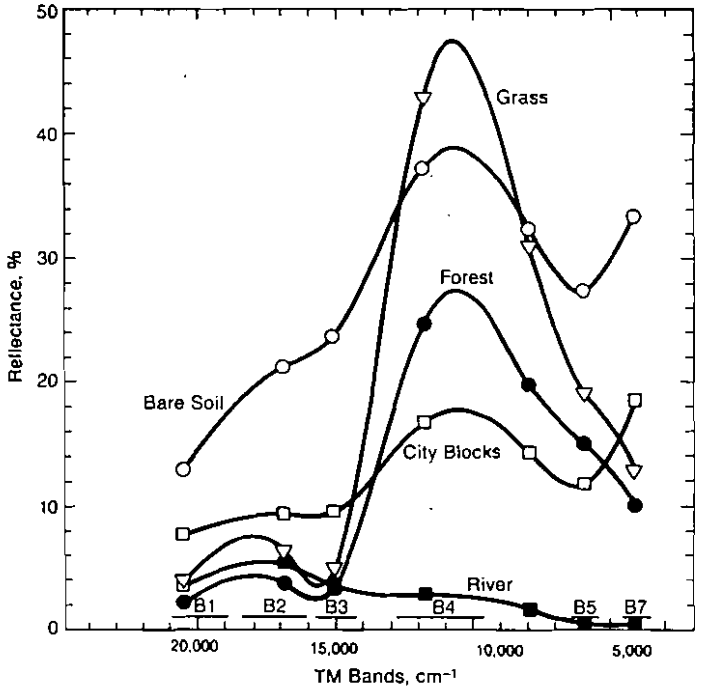

Figure 3. Derived spectral reflectances of five surface types (nadir view) are presented with TM spectral bands.

Downloaded by [171.67.216.21] at 13:17 26 April 2014

Table 3. Net solar radiation absorbed by surface categories.

Date	2 Nov	18 Mar	24 Mar	9 Aug	26 May	24 June
			(Wm^{-2} at 9.33 am local time)			
Incident solar flux	310	334	448	610	611	631
Net absorbed by						
Bare soil	254	256	340	437	427	440
Grass	267	273	366	478	470	485
Urban	285	299	400	532	528	544
Forest	284	296	397	528	523	541
River	304	327	438	592	593	611

to determine the net radiation intakes by various surface types. And the net solar radiation absorbed by the five surface categories according to the one minus albedo formula given in (2) are listed in table 3. The table lists the solar energy intakes of five different surface materials as a function of the vertical component of the incident sunlight.

One of two interesting facts emerge from these detailed spectral reflectances. Vegetative areas, in general, are good absorbers of solar radiation in spite of their high reflectivity in the near-IR region. It would appear that the strong near-IR reflectance, even in the growing season, is offset by a strong absorption taking place in the blue region. This absence of strong season fluctuation can be interpreted as proof that the net solar energy going into the photosynthetic process in the plant canopy is negligibly small even though substantially large amounts of thermal energy are consumed in evapotranspiration.

Secondly, one can determine that the radiational properties of an urban area can be characterized as a compromise between bare soil and woodland. The absorptional profile of Washington, DC, closely resembles that of bare soil, according to figure 3. However the total profile has been shifted toward the low reflectances of a forest canopy, indicating there are fair amounts of sidewalk, trees along the boulevards and shadows among the buildings.

5. Thermal analysis of an urban area

The concept of inferring the thermal properties of a surface using infrared radiometric measurement in conjunction with a surface model is widely used to study evapotranspiration in agricultural fields (Soer 1980, Seguin and Itier 1983; Vidal and Perrier 1989), soil moisture in bare soil (Idso *et al.* 1975) and rock and mineral formations via thermal inertia (Kahle 1977). However over heterogeneous surface such as an urban-rural complex, a commonly accepted thermal model that can be applied across the entire scene to partition the surface energies is not readily available. Carlson *et al.* (1981) confronted this problem in their urban heat island study by instituting a couple of effective surface parameters which govern the temperature response. Their model divides the energy components into sensible heat flux and latent energy of evaporation as each term was parameterized using eddy diffusibility and a moisture availability factor. Two surface temperature observations measured by HCMM (Heat Capacitance Measurement Mission) at the times of maximum and minimum diurnal temperatures, were applied to infer the surface

Downloaded by [171.67.216.21] at 13:17 26 April 2014

energy fluxes of an urban area. In this TM analysis, the amplitude of the diurnal thermal cycle were given by the difference between the pre-dawn air temperature and the 9.33 am (local time) satellite brightness temperature. Each set's accumulated energies were calculated by numerical integration of a SZA function for the duration of solar insolation. An important assumption is that the surfaces will cool down to approximately the pre-dawn climatological temperature being measured at 1 m above the ground by the National Weather Service. In a strict sense, the brightness temperature being measured by satellite needs to be corrected for the surface emissivity (Kimes 1980, and Brunet *et al.* 1991) and the vertical temperature gradient of the atmosphere. However, for brevity, the emissivity of the ground is set equal to 1·0 and the contribution of $T_{(atm)}$ for all six cases was assumed constant.

Partitioning of the surface energies was carried out largely following the Penman-Montieth Model described by Bevan in 1979, and Martin *et al.* in 1989. The complexities of quantitizing the energy transfer process were further compounded by the fact that the original P-M model which is a one-dimensional evapotranspiration model, well accepted as a prediction model for vegetation canopy, must be stretched to accommodate the interacting terms of the moisture content in non-vegetation areas such as bare-soil or water.

The original expression for evaporation from a plant canopy is given as

$$E=\frac{s(SRI+S)+\{\delta_a C_p[V_p(T_{sfc-Tair})]/R_a\}}{L\{s+[\gamma((R_a+R_c)/R_a)]\}} \tag{3}$$

where: E = evaporative water loss from the surface, L = latent heat of vaporization of water, s = slope of the specific humidity temperature curve, SRI = available energy short wavelength radiation intake, S = soil heat flux, δ_a = density of air, C_p = specific heat of air, $[V_p(T_s-T_a)]$ = specific humidity deficit (SHD). Saturation vapour pressures at the temperatures of surface and the air immediately above, γ = psychometric constant, R_a = effective aerodynamic resistance to the transport of water vapour from the surface to the air, R_c = canopy resistance.

The parametric data required are values of R_a and R_c, the external aerodynamic and canopy resistances, respectively. The external aerodynamic resistance, R_a, was derived using the general heat transfer equation as aerodynamic transfer coefficients for heat and moisture area treated nearly equal (Dickinson 1983).

$$H_{(sens)}=\{[\delta_a C_p(T_s-T_a)]/R_a\} \tag{4}$$

The model requires the knowledge of the windspeed in addition to available solar energy and temperature profiles. The $H_{(sens)}$ is caused by exposure of surfaces to the wind and its rate of heat transfer, at a given wind condition, is proportional to the temperature differences between the surface and air. In order to determine R_a, a second assumption was made: only negligibly small amounts of evaporation are available from bare soil or concrete pavements. Thus the LE terms for bare soil are initially less than 5 per cent of the SRI as κ in (5) has been set to 0·95. This approach is similar to an atmospheric effect correction where the water leaving radiances in the near-IR region are assumed to be near zero. This leaves the surface heat flux for bare soil to be determined as a solution of the surface energy balance.

$$H_{(sens)}=\kappa^*[SRI_{(bare\ soil)}]-OLR \tag{5}$$

where the κ is set to 0·95. By inverting (4) for bare soil, R_a values for the six dates were obtained. This parameterization of external aerodynamic resistance allows one

Downloaded by [171.67.216.21] at 13:17 26 April 2014

to carry out the rest of the LE computations for the remaining surfaces using the expression given in (3) is balanced with appropriate R_c value. Because the daytime heating of the surfaces were estimated by the time lapse temperatures of pre-dawn to satellite overpass, the SHD term in (3) pertains to a specific humidity deficit defined by the temperature change of two types of temperature measurements.

This method of inverting the analytical expression by inputting multi-data sets, can provide solutions by simplifying some of the problems although the derived parameters may no longer bear original physical significance of the expression. For instance, the effective R_a, in this case, should be construed as an external turbulence factor which relates to an unspecified transition layer between the air and the surface across which diffusive fluxes are passed from the surface to the turbulent layer. In the case of R_c, the term should be taken as the effectiveness of the canopy to transport water from below to the canopy surface. There is a variation in molecular flow regardless whether the surface types are vegetation or non-vegetation. Therefore, in a plant leaf, it is a function of the stomatal resistance. Water surfaces would have the condition of $R_c=0$ and large values are expected for dry bare soil.

In table 4, a listing of surface energy components are listed in terms of reflectances, total solar radiation absorbed, sensible heat flux, the outgoing long-wave radiation, and the latent heat of evaporation. Even though the content of the table lists the energies in fluxes, the values of the table are by no means meant to represent quantization in absolute terms but should be construed as a relative measurement.

Sensible heat fluxes are predominant in bare soil, especially in winter, and in all cases, evaporation increases with the increasing sun-light as the warming brings out more moisture from the surface. A linear regression analysis of the derived energy components with respect to the surface reflectance yields approximate but surprisingly simple correlations.

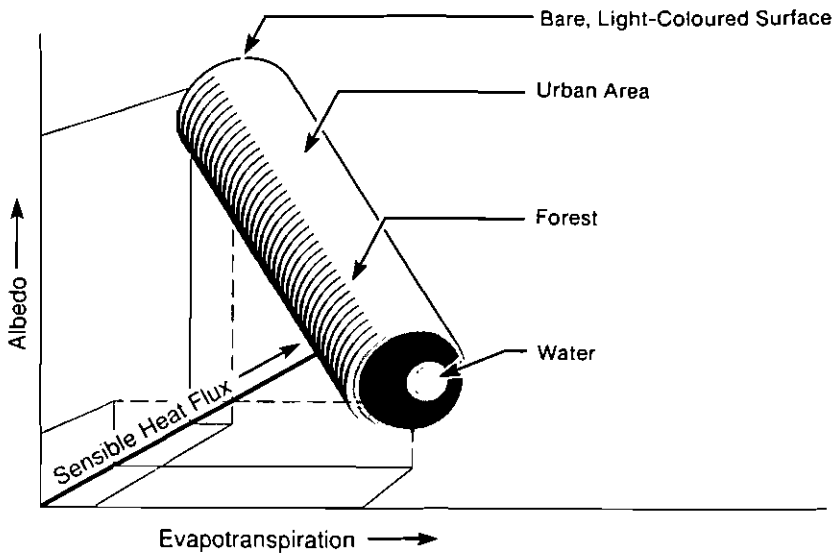

Figure 4. Surface energy compositions, *ISR*, *LE* and $H_{(sens)}$, for surface types in three-dimensional space. Arrows indicate areas where some types of surface materials might occur.

Downloaded by [171.67.216.21] at 13:17 26 April 2014

Table 4. A listing of surface thermal energies according to surface types and seasons.

Date (SZA in deg)	Type	Refl.	*SRI* $W^1 m^{-2}$	$H_{(sens)}$ $W^1 m^{-2}$	*LE* $W^1 m^{-2}$	*OLR* $W^1 m^{-2}$
2 November 1982	Bare soil	0·18	162	106	4	52
(57·5)	Grass	0·14	170	63	55	50
	Urban	0·08	182	71	57	50
	Forest	0·08	181	63	69	50
	River	0·02	194	15	113	47
18 March 1989	Bare soil	0·23	165	117	4	53
(47·2)	Grass	0·18	176	60	68	48
	Urban	0·10	193	86	53	50
	Forest	0·11	191	89	53	50
	River	0·02	211	24	126	47
24 March 1984	Bare soil	0·24	216	150	14	52
(44·9)	Grass	0·18	233	98	86	47
	Urban	0·11	255	116	88	49
	Forest	0·11	253	116	90	49
	River	0·02	279	42	162	43
9 August 1989	Bare soil	0·28	279	201	9	70
(33·3)	Grass	0·22	303	120	118	61
	Cornfield	0·19	315	101	154	60
	Urban	0·13	338	156	114	64
	Forest	0·13	335	97	175	58
	River	0·03	376	97	219	58
26 May 1985	Bare soil	0·30	279	197	14	69
(27·9)	Grass	0·23	308	88	156	58
	Urban	0·14	346	133	149	63
	Forest	0·14	343	76	206	57
	River	0·05	380	46	274	54
24 June 1987	Bare soil	0·30	288	179	39	71
(27·3)	Grass	0·23	318	101	155	61
	Urban	0·14	357	126	164	64
	Forest	0·14	354	78	217	58
	River	0·01	413	79	273	58

$$H_{(sens)}\,(\mathrm{W\,m^{-2}}) = 0{\cdot}52\mathrm{F}\,(\mathrm{g}) - 85 + 380\rho(r^2 = 0{\cdot}61) \quad (6)$$

$$OLR = 0{\cdot}04\mathrm{F}\,(\mathrm{g}) + 37 + 33\rho(r^2 = 0{\cdot}62) \quad (7)$$

$$LE = 0{\cdot}97\mathrm{F}\,(\mathrm{g}) - 108 - 600\rho(r^2 = 0{\cdot}76) \quad (8)$$

The r^2s denote the critical correlation coefficients. The above relationships are significant in that the degree of enhancement of both long and short wave-length fluxes leaving the surface into the atmosphere due to changes in surface reflectance can be given as the function of reflectance and solar radiation incident. Figure 4 pertains to a comprehensive view of the energy balance given in the table and is presented in three-dimensional scatter volume with arrows indicating volumes where certain types of Earth surface might occur.

Downloaded by [171.67.216.21] at 13:17 26 April 2014

6. Surface radiation budget imagery

The concept of incorporating surface energy balance into high spatial resolution maps offers a number of practical applications. For instance, a false colour image which scales the three energy vectors of figure 4 may yield a picture of the surface energy status of an urban area or water stress status in agricultural fields.

Image processing procedures which convert the raw radiances of TM imagery to surface radiation budget imagery were carried through by largely following the analytical procedures given in equations 1–5 in the following steps:

(1) Initially, multi-spectral images of visible and near-IR channels were converted to a normalized reflectance image. The solar energy intake imagery was created according to the relationships of one minus albedos given in (2).
(2) The thermal band-6 images were converted to sensible flux images using the formula given in (4) and another set of band-6 images were converted into *OLR* imagery.
(3) A pixel by pixel subtraction of sensible heat flux and *OLR* imagery from the one minus albedo input function imagery of first step yields the *LE* imagery.

The energy balance status of Washington, DC, on 9 August 1989 is depicted by such a surface radiation budget approach in figure 5. The colour scheme assigns the sensible heat fluxes, albedos, and evaporations to RGB channels respectively. For comparison, a conventional reflectance image of TM bands 1, 3 and 4 is presented in figure 6.

The surface radiation budget image is interesting in that the product not only displays detailed structure of microscale climate but also provides information on the relative moisture content of the surface. Vegetation areas can be further broken down to woodlands, tall, and short grass as each respectively takes up blue, green and orange according to the evapotranspiration rates.

In figure 7, the formation of the urban heat island in Washington, DC, on 24 June 1987 at 9.33 am is presented in three-dimensional profile. The deep trough encircling the city is a low temeprature belt being formed by Rock Creek Park, the Potomac and Anacostia Rivers. Relatively flat urban heat canopy is already forming in the morning hours of the summer. A large hump in the left upper corner is in the areas of Bethesda, MD, a burgeoning satellite city with a cluster of high rise buildings. One possible scenario for DC residents may be attributed to the fact that a convective warm air mass rising over the city may be drawing moisture from surrounding rivers and forests making the city extremely humid and hot by the afternoon (Harneck and Landsberg 1975). A recent analytic and numerical study (Baik 1991) indicates that the updraught circulation cell, which is produced by the nonlinear processes, on the downstream side of the heat island is partly responsible for precipitation enhancement observed downwind of the heat island.

7. Discussions

Existing theories on the occurrence of urban/rural contrast are diverse as many factors contribute to the phenomena. Early work by Duckworth and Sandberg (1954) described the formation of the urban heat island as anthropogenic heat generation being trapped among buildings. Bach and Patterson (1969) pointed out the effects of atmospheric radiance as one of the causes as the city can experience increased down-welling radiation fluxes due to atmospheric pollution. However, the

Downloaded by [171.67.216.21] at 13:17 26 April 2014

Downloaded by [171.67.216.21] at 13:17 26 April 2014

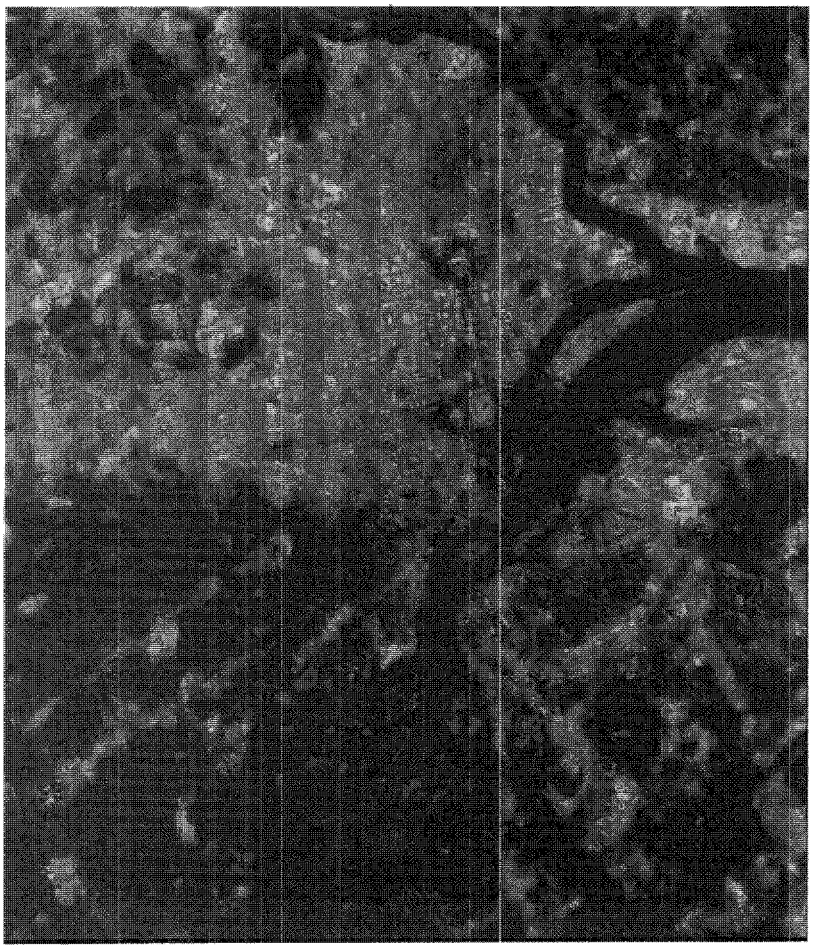

Figure 5. The energy balance of the metropolitan DC area on 9 August 1989 is presented in false colour as sensible heat flux, albedos and evaporation, assigned to RGB channels respectively.

Figure 6. False colour image of DC on 9 August 1989. TM bands 1, 3 and 4 are assigned to RGB respectively.

Downloaded by [171.67.216.21] at 13:17 26 April 2014

work of Oke and Fuggle (1972) showed that the feedback of long wavelength radiation from the atmosphere to the surface is small, exhibiting negligible urban/rural differences. Terjung *et al.* (1970) studied the presence of variations in the atmospheric temperature over a section of Los Angeles. Interpretations on the effect of albedo changes on surface temperature are also diverse. Among others, Oguntoyinbo (1970), based on his portable solari-albedometer measurements, reported that reduced albedo in the city which results in increased urban heating. Adebayo (1990), based on his recent automobile traverse measurements, reported that the urban areas exhibit slightly smaller albedo than their rural counterpart, yet the city contains a larger net balance of the radiations.

Analogous model studies on the sensitivity of climate to surface albedo and

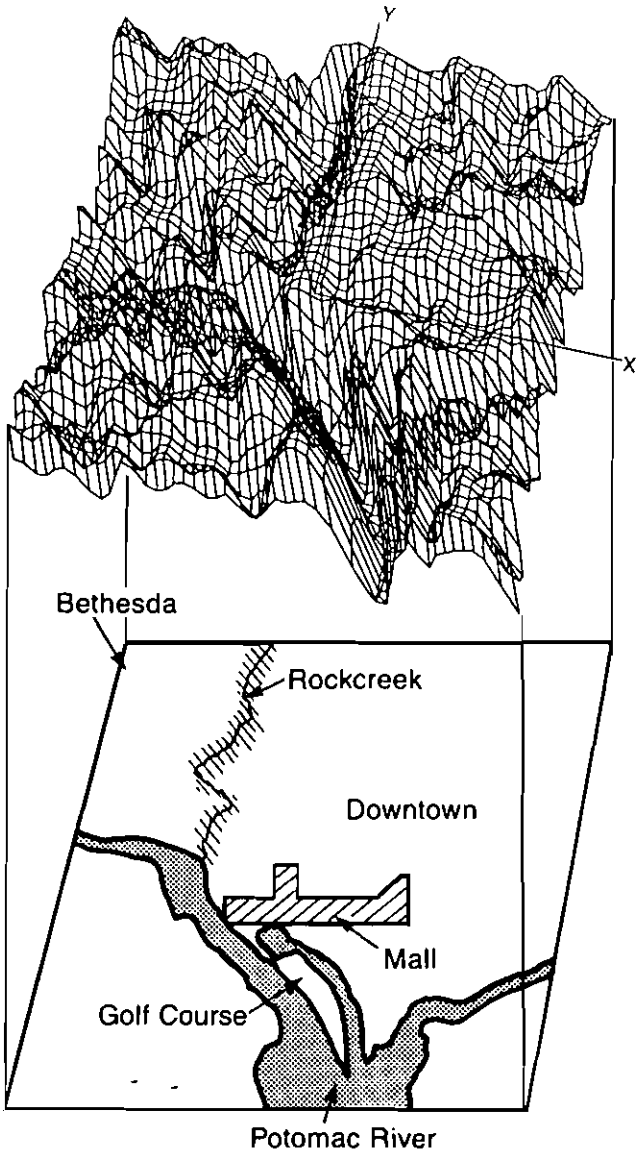

Figure 7. Three-dimensional profile of urban heating taking place in Washington, DC by 9.33 in the morning (24 June 1987).

Downloaded by [171.67.216.21] at 13:17 26 April 2014

moisture content are also available from large scale modelling of Charney (1975), Charney *et al.* (1977), Laval (1986), and Sud and Fennessy (1982). In principle, most models agree that a perturbation of albedo can cause climatic change such as surface heating or increased precipitation. Charney (1975) initially reported that increases in albedo reduced absorption of solar radiation causing a radiative heat sink. However, in his later model (1977) different results were reported as the evaporation rates were incorporated with the albedo influences. The results of Laval in 1986 are more comprehensive: when albedo increases in semi-arid areas, the net radiative heating of surfaces decrease and so did the rainfall. From this, one can surmise that there is an ambiguity in determining the role of surface albedos as an interacting parameter in general circulation models.

The results of this TM imagery analysis do not reinforce or contradict any of the existing interpretations of the phenomenology by others. However, it is to be noted that the semi-empirical relationships given in equations 6-8 are based on the observational data of thousands of pixels across the several types of surfaces. Therefore the quantitative relationship can be immediately put into an analysis of both long- and short-wave radiation fluxes leaving the surface into the atmosphere due to the changes in surface reflectance.

However, the urban heat island phenomenon presented here may belong to a case of albedo anomalies where the *city blocks* seem to demonstrate smaller than expected albedos. Even though spectral signature of the *city blocks* would appear to be closely that of non-vegetation surface, the albedo in broad band structure is almost on the level of forest. Perhaps one may attribute this to the fact that large buildings and boulevards of the city might be contributing to the formation of large shadows. Derived relations between the SRI and surface temperature for five surfaces in figure 8 demonstrate that surface heating is most in bare soil and there is a difference of 20° against surrounding rural environment. Urban heating in Washington, DC begin to form by mid-morning in summer and a difference of 10° can be expected against adjacent *Rock Creek Park* forest.

There is an inverse relationship between the albedo and latent heat of evaporation. Thus excessive surface heating can be attributed to a reduction in local evaporation. Figure 8 curves also reinforce the role of moisture content as the retarding force in surface heating. The derived relationships between solar intakes and temperature are in non-linear regressions and this is consistent with the presence of a relatively sharp break-point in diurnal soil temperature profiles reported by McCumber and Pielke in 1981. The phenomenon is related to soil moisture content and its threshold temperature.

From this one can almost construct a scenario for the formation of an urban heat island. City surface under intense solar radiation will seek a heat sink. For instance, the evaporation, or moisture availability, is available heat sink in retarding rapid temperature rises. When evaporation route is not available, alternatively the heat is transferred to the air as sensible heat flux. Sensible heat flux conditions require the surface temperature to be higher than the air and daylight heating in the city exactly matches these conditions. A large sensible heat flux means large temperature rise of the air above which eventually leads to an increased warmth of the city atmosphere. In regard to the inverse relationship between the urban heating and absorption, it should be pointed out that by nature, the water is one of the better solar radiation absorbers and the drier tbe surface material, it tends to reflect the sunlight displaying high albedo nature.

Downloaded by [171.67.216.21] at 13:17 26 April 2014

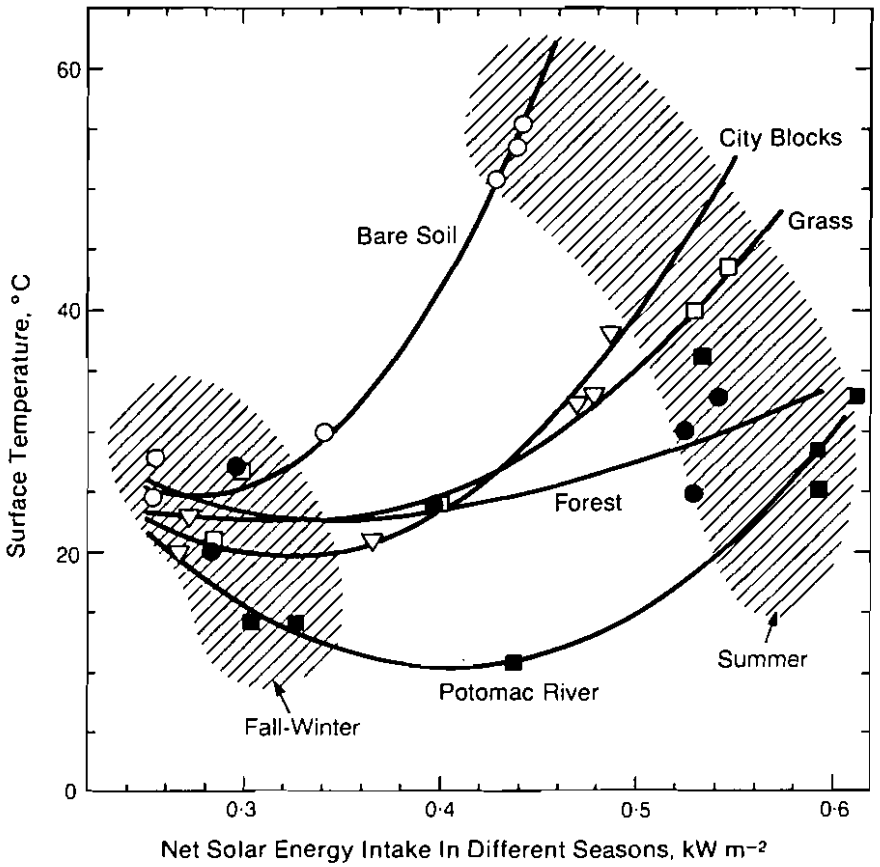

Figure 8. The net radiation absorbed versus the surface temperature for different surfaces with smoothed non-linear regression fits.

8. Summary

An urban heat island is a regional climate phenomenon. Yet, in many aspects, it is a microcosm of the Earth's climate over the land where both soil albedo and moisture availability become important components of overall boundary forcing and its feedback effects. An analysis of empirical data indicates that the roles of surface albedos and moisture availability to surface energy balance can be approximated in simple linear regressions in spite of the land surface's temporal and spatial variability. Further refinement and validation will be needed based on wider observational data. The goal of high resolution local model is not only for applications in regional climatology but also for validation of such a model from local scales up to GCM grid sizes.

Acknowledgments

The author wishes to thank Drs W. L. Barnes, R. S. Fraser and S. H. Melfi with whom several interesting conversations on atmosphere, sensor, water vapour content and surface reflectance had taken place during the preparation of this article.

Appendix A

The 5960 deg K black body radiations which fall within each TM spectral band was calculated by the Planck's radiation functions. The cumulative spectra radiance,

Downloaded by [171.67.216.21] at 13:17 26 April 2014

D, of a black body within the spectral band from λ to $\lambda=0$ can be given as

$$D=\frac{\int_0^{\lambda} N_\lambda d_\lambda}{\int_0^{\infty} N_\lambda d_\lambda}$$

where

$$N_\lambda=\frac{C}{\lambda^5 \exp\left(c^2/(\lambda T)-1\right)}$$

The subtraction of $D_{(upper)}$ from $D_{(lower)}$ for band i gives the radiance, N_i, of a blackbody within a broad spectral band i. F° is the solar constant 1352 W m^{-2}.

$$N_i=F^\circ\ (D_{(lower)}-D_{(upper)})$$

TM band	Width of band (micron)	Fraction D $(D_{(lower)}-D_{(upper)})$	Blackbody radiation N_i $F^\circ(D_{(lower)}-D_{(upper)})$
B 1	0·45–0·52	0·288–0·195	127
B 2	0·52–0·615	0·409–0·288	163·2
B 3	0·615–0·71	0·514–0·409	141·6
B 4	0·71–0·9	0·67–0·514	211·3
B 4-5	0·9–1·55	0·897–0·67	305·8
B 5	1·55–2·08	0·951–0·897	73·0
B 7	2·08–2·35	0·985–0·951	46·37
Total			1068 W m^{-2}

References

ADEBAYO, Y. R., 1987, Short communication: a note on the effect of urbanization in Ibadan. *Journal of Climatology*, **7**, 185–192.

ADEBAYO, Y. R., 1990, Aspect of the variation in some characteristics of radiation budget within the urban canopy of Ibadan. *Atmospheric Environment*, **24B**, 9–17.

BACH, W., and PATTERSON, W., 1969, Heat budget for polluted layers of the urban environment. *Proceedings of the Association of American Geographers*, **1**, 7–11.

BAIK, J. J., 1992, Response of a stably stratified atmosphere to low-level heating—an application to heat island problem. *Journal of Applied Meteorology*, In Press.

BEVAN, K., 1979, A sensitivity analysis of the Penman-Montieth actual evapotranspiration estimates. *Journal of Hydrology*, **44**, 169–190.

BRUNET, Y., PAW-U, K. T., and PRIVOT, L., 1991, Using the//adiative surface temperature in energy budget studies over plant canopies. *Proceedings of 5th International Colloquium on Physical Measurements and Signatures in Remote Sensing, ESA SP-319* (Paris: E.S.A.), pp. 557–560.

CARLSON, T. N., DODD, J. K., BENJAMIN, S. G., and COOPER, J. N., 1981, Satellite estimation of the surface energy balance, moisture availability and thermal inertia. *Journal of Applied Meteorology*, **20**, 67–87.

CARLSON, T. N., 1986, Regional-scale estimates of surface moisture availability and thermal inertia using remote thermal measurements. *Remote Sensing Review*, **1**, 197–244.

CHARNEY, J. G., 1975, Dynamics of deserts and drought in the Sahel, *Quarterly Journal of the Royal Meteorological Society*, **101**, 193–202.

CHARNEY, J. G., QUIRK, W. J., CHOW, S., and KORNFIELD, J., 1977, A comparative study of the effects of albedo change on drought in semi-arid regions. *Journal of Atmospheric Science*, **34**, 1366–1385.

Downloaded by [171.67.216.21] at 13:17 26 April 2014

DICKINSON, R. E., 1983, Land surface processes and climate—surface albedos and energy balance. *Advances In Geophysics*, **25**, 305-353.

DUCKWORTH, F. S., and SANDBERG, J. S., 1954, The effect of cities upon horizontal and vertical temperature gradients. *Bulletins of American Meteorological Society*, **35**, 198-207.

HARNACK, R. P., and LANDSBERG, H. E., 1975, Selected cases of convective precipitation caused by the metropolitan area of Washington, D.C. *Journal of Applied Meteorology*, **14**, 1050-60.

IDSO, S. B., SCHMUGGE, T. J., JACKSON, R. D., and REGINATO, R. J., 1975, The utility of surface temperature measurements for the remote sensing of surface soil water status. *Journal of Geophysical Research*, **80**, 3044-3049.

KAHLE, A. B., 1977, A simple thermal model of the Earth's surface for geologic mapping by remote sensing. *Journal of Geophysical Research*, **82**, 1673-1680.

KIM, H. H., and ELMAN, G., 1990, Normalization of satellie imagery. *International Journal of Remote Sensing*, **8**, 1331-1347.

KIM, H. H., 1991, Urban heat island. *Proceedings of 5th International Colloquium on Physical Measurements and Signatures in Remote Sensing*, ESA SP-319 (Paris: E.S.A.), pp. 521-525.

KIMES, D. S., IDSO, S. B., PINTER, JR., P. J., REGINATO, R. J., and JACKSON, R. D., 1980, View angle effects in the radiometric measurement of plant canopy temperatures. *Remote Sensing of Environment*, **10**, 273-284.

LANDSBERG, H. E., 1970, Man-made climate changes. *Science*, **170**, 1265-1274.

LANDSBERG, H. E., and MAISEL, T. N., 1972, Micrometeorological observations in an area of urban growth. *Boundary-Layer Meteorology*, **2**, 365-370.

LAVAL, K. M., 1986, General circulation model experiments with surface albedo changes. *Climate Change*, **11**, 91-102.

MCCUMBER, M. C., and PIELKE, R. A., 1981, Simulation of the effects of surface fluxes of heat and moisture in a meso-scale numerical model 1. Soil layer. *Journal of Geophysical Research*, **86**, 9929-9938.

MARTIN, P., ROSENBERG, N. J., and MCKENNEY, M. S., 1989, Sensitivity of evapotranspiration in a wheat field, a forest and a grassland to changes in climate and direct effect of CO_2. *Climate Change*, **14**, 117-151.

NUNEZ, M., SKIRVING, W. J., and VINEY, N. R., 1987, A technique for estimating regional surface albedos using geostationary satellite data. *Journal of Climatology*, **7**, 1-11.

OGUNTOYINBO, J. S., 1970, Reflection coefficient of natural vegetations, crops, and urban surfaces in Nigeria. *Quarterly Journal of Royal Meteorological Society*, **96**, 430-41.

OKE, T. R., 1976, The distribution between canopy and boundary layer urban heat islands. *Atmosphere*, **14**, 268-276.

OKE, T. R., and FUGGLE, R. F., 1972, Comparison of urban/rural counter and net radiation at night. *Bondary-Layer Meteorology*, **2**, 290-308.

SEGUIN, B., and ITIER, B., 1983, Using midday surface temperature to estimate daily evapotranspiration from satellite thermal IR data. *International Journal of Remote Sensing*, **4**, 371-383.

SOER, G. J. R., 1980, Estimation of regional evapotranspiration and soil moisture conditions using remotely-sensed crop surface temperatures. *Remote Sensing of Environment*, **9**, 27-45.

SUD, Y. C., and FENNESSY, M., 1982, A study of influence of surface albedo on July circulation in semi-arid regions using the glas GCM. *Journal of Climatology*, **2**, 105-125.

TERJUNG, W. H., and LOUIE, S. S.-F., 1973, Solar radiation and urban heat islands. *Annals of the Association of American Geographers*, **63**, 181-207.

THOMPSON, K., 1981, The questions of climatic stability in America before 1900. *Climate Change*, **3**, 227-241.

VIDAL, A., and PERRIER, A., 1989, Analysis of a simplified relation for estimating daily evapotranspiration from satellite thermal IR data. *International Journal of Remote Sensing*, **10**, 1327-1337.

VITERITO, A., 1989, Changing thermal topography of the Baltimore-Washington corridor: 1950-1979. *Climate Change*, **14**, 89-102.

Downloaded by [171.67.216.21] at 13:17 26 April 2014